Liquid Precursor Plasma Spraying: Modeling the Interactions Between the Transient Plasma Jet and the Droplets

C. Marchand, C. Chazelas, G. Mariaux, and A. Vardelle

(Submitted March 12, 2007; in revised form June 27, 2007)

Plasma spraying using liquid feedstock makes it possible to produce thin coatings (<100 μm) with more refined microstructures than in conventional plasma spraying. However, the low density of the feedstock droplets makes them very sensitive to the instantaneous characteristics of the fluctuating plasma jet at the location where they are injected. In this study, the interactions between the fluctuating plasma jet and droplets are explored by using numerical simulations. The computations are based on a three-dimensional and time-dependent model of the plasma jet that couples the dynamic behaviour of the arc inside the torch and the plasma jet issuing from the plasma torch. The turbulence that develops in the jet flow issuing in air is modeled by a large Eddy simulation model that computes the largest structures of the flow which carry most of the energy and momentum.

1. Introduction

During the last decade, many plasma spraying-based techniques (Ref 1-8) using liquid feedstock have been developed to create nanostructured coatings. Indeed, a decrease in the grain size results in a significant increase in the volume fraction of grain boundaries or interfaces that strongly influences the chemical and physical properties of the material.

These techniques use either suspensions of fine particles or solutions. The latter are made by dissolving of metal salts or organometallic precursors or liquid metal precursors in a solvent. The suspension precursors consist of nano- or micro-sized particles, aqueous or organic solvents and effective dispersing agents that develop repulsive forces and prevent the aggregation of particles. In both cases, the liquid feedstock must be stable and homogeneous with a low viscosity.

C. Marchand, C. Chazelas, G. Mariaux, and **A. Vardelle**, Laboratoire Sciences des Procédés Céramiques et Traitements de surface, University of Limoges, ENSIL, Limoges, France. Contact e-mail: armelle@ensil.unilim.fr.

When the spray techniques use conventional DC plasma torches, the feedstock is generally injected perpendicularly to the plasma jet axis in liquid jet or droplet form that are subjected to breakup and evaporation in the hot gas flow. Once the solvent is evaporated, the fine particles contained in the suspension droplets are heated and accelerated and impact, in a molten or semi molten state, on the substrate, depending on the particle trajectories as in conventional plasma spraying. In the case of dissolved chemicals, the precursor undergoes rapid breakup and evaporation in the plasma followed by precipitation and pyrolysis. The mechanisms that control the thermal and chemical treatment are also critically dependent on the trajectories of the droplets in the plasma jet (Ref 6).

Research studies (Ref 1-7) carried out to understand the mechanisms governing coating deposition in liquid precursor plasma spraying have shown that this technology is faced with two main difficulties: (i) the injection and penetration of the liquid feedstock into the fluctuating gas flow and (ii) the heterogeneous behaviour of the droplets in the core and periphery of the plasma jet. Similar problems are encountered in conventional powder plasma spraying but in liquid precursor plasma spraying they are aggravated (i) because of the low specific density of droplets that makes them very sensitive to fluctuations of the plasma jet and possible drifts in the nominal conditions of the process, and (ii) because of the fragmentation of the droplets in smaller droplets and the intense evaporation undergone by the liquid precursor in the plasma jet.

This study deals with the injection of droplets in a plasma jet and uses a three-dimensional (3D) and time-dependent model of the plasma jet issuing in air in conjunction with a large Eddy simulation (LES) turbulence model to examine the influence of the arc voltage fluctuation amplitude and frequency on the time-evolution of the plasma jet flow fields and droplet injection. The LES

model is becoming a standard tool to study the dynamics of turbulent plasma flames but has not been applied to plasma jets. It makes it possible to compute the transient large-scale structures of the flow that contain most of the energy and momentum and are naturally embedded in the governing equations while the smaller dissipative scales have been found to be more universal, and hence are more easily modeled by conventional turbulence models. Model projections are compared with experimental measurements and predictions of the 3D model when using k–ε turbulence model. The latter that is based on the isotropic eddy viscosity concept and Reynolds Averaged Navier-Stokes (RANS) modeling approach is by far the most popular and most widely used turbulence model. It consists of two transport equations. The first transported variable is the specific turbulent kinetic energy, k, and the second variable is the turbulent dissipation, ε, that determines the scale of the turbulence.

2. Liquid Feedstock Injection in the Plasma Jet

The liquid is commonly injected into the plasma jet either by pneumatic or mechanical injection. In the former technique, the liquid is atomized by a gas jet into droplets that have a broad size (5-100 μm in diameter) and velocity distribution (5-100 m s^{-1}). The sizes of the atomized droplets depend on the pressure in the liquid reservoir, atomisation gas flow rate and nozzle diameter. Owing to the distribution in droplet sizes and velocities, not all the droplets penetrate the same region of the plasma flow and, thus, undergo different thermal and chemical treatment. In addition, the colder and denser atomisation gas can perturb the plasma flow.
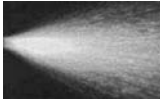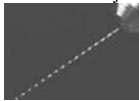
In mechanical injection systems, the liquid is fed from a pressurized reservoir through a precision nozzle (50-150 μm in diameter). The geometry of the nozzle flow depends on the geometry of the nozzle and reservoir pressure. The liquid stream can undergo a primary break-up, caused by waves that form on the surface of the stream after it has travelled some distance from the nozzle outlet plane. These waves grow in amplitude while maintaining a constant wavelength.

A transition occurs as the waves form more of a localized 3D structure, most likely dominated by surface tension effects. Large-scale breakup of the sheet takes place rapidly at this transition point. The use of an additional system that delivers constant pressure pulses (Ref 2, 7) makes it possible to break up the liquid stream into mono-sized and equidistant droplets and to independently control the liquid flow rate and size and velocity of droplets. Table 1 summarizes the characteristics of these various systems of injection.

Irrespective of the injection system, the liquid stream or droplets undergo fragmentation and evaporation as they enter the plasma jet. Calculations of droplet fragmentation by using a force balance between the drag force and surface tension force showed that the fragmentation time of droplets 50-300 μm in diameter was shorter by 2-3 orders of magnitude than the vaporisation time (Ref 3). Therefore, the fragmentation process will condition to a great extent the trajectory and, thus, the heat and chemical treatment of the final droplets.

The diameter of the fragmented droplets is inversely proportional to the plasma momentum density $\rho.v^2$. As the plasma jet issuing from conventional plasma torches is characterized by time- and space-variation, the diameter of droplets after break-up will depend on the time and location where they are injected. Indeed, in the section of

Table 1 Characteristics of the systems commonly used to inject liquid feedstock in plasma jets

Injection system	Photograph of the nozzle flow		Operating parameters	Droplet main characteristics
Pneumatic (Ref 1, 3, 5)			Pressure in tanks (1-8 bars) Atomisation gas flow rate Diameter of injector nozzle (150 μm)	$d \sim$ 5-40 $\Phi \sim$ 5-100 $v \sim$ 5-100
Mechanical (Ref 2, 3, 7)	Linear liquid jet	Magnetrostrictive drive rod injector	Pressure in tanks (1-8 bars) Diameter of injector nozzle (150 μm)	$d \sim$ 10-30 $\Phi \sim$ 300 $v \sim$ 10-35
	Ink jet printer		Pressure in tanks (1-5 bars) Diameter of injector nozzle (50 μm)	$d \sim$ 1-3 $\Phi \sim$ 100 $v \sim$ 10-20

d (mL min^{-1}) is the liquid flow rate; Φ (μm) and v (m s^{-1}) are the droplet diameter and velocity, respectively

the flow where the liquid is injected, the temperature increases from 300 K in the periphery of the plasma flow up to 10,000-12,000 K in the core of the flow and the velocity from 0 to 1,000-2,000 m s^{-1}. Also, the random motion of the arc inside the nozzle results in time-variation in the arc voltage V_{arc}. These fluctuations can be characterized by the ratio of the amplitude variation of arc voltage ΔV_{arc} to the time-averaged voltage $V_{average}$. This ratio varies from 0.25 in the best conditions of the takeover arc operation mode to 1.5 in the worst conditions of the restrike mode (Ref 9). These arc fluctuations protect the anode wall from erosion but they result in fluctuations in the enthalpy input to the plasma-forming gas in unison with the voltage fluctuations. The relative variation of the plasma velocity at the nozzle exit may be as high as the ratio $\Delta V_{arc}/V_{average}$; the variation of temperature is much lower since at temperature ranges between 9,000 and 12,000 K, heat is stored in the gas species in the form of ionisation energy that acts as a thermal inertia wheel and dampens the plasma temperature variation.

In the plane of injection of the liquid, the momentum density of the plasma jet $\rho.v^2$ varies drastically with time and the fragmentation process fluctuates accordingly, as observed by Etchart-Salas et al. (Ref 4). In order to do this, they used a fast shutter camera (Oseir's SprayWatch®) coupled with a laser flash at 808 nm and triggered by a defined instantaneous voltage level of the plasma torch. They showed that the voltage fluctuations amplitude, which was increased by shifting from argon-helium to argon-hydrogen as plasma-forming gas, strongly affects the fragmentation of the liquid stream. They also observed a significant variation in the distribution of the droplets trajectories as the volume in which the droplets were travelling seemed to contract or expand at the rate of the arc fluctuation frequency.

3. Operating Conditions and Methodology of the Numerical Study

The objective of the numerical simulations is to investigate *separately* the effect of the amplitude of variation and frequency of the arc voltage on liquid injection in the plasma jet. The methodology followed in this study is the following:

1. Selection of a reference case: computations of the arc dynamics *inside the plasma torch* with a magneto hydrodynamic (MHD) model (Ref 10) and computation of the plasma jet issuing from the torch. These computations were performed with a plasma torch of 6-mm nozzle diameter, plasma-forming gas composed of 45 slm of argon and 15 slm of hydrogen and arc current of 600 A. Under these conditions, the arc operates in the restrike mode in an actual plasma torch, because of the high gas flow rate and content of hydrogen (25%) in the plasma-forming gas. The computations made it possible to predict the time-variation of arc voltage (see Fig. 1) and enthalpy
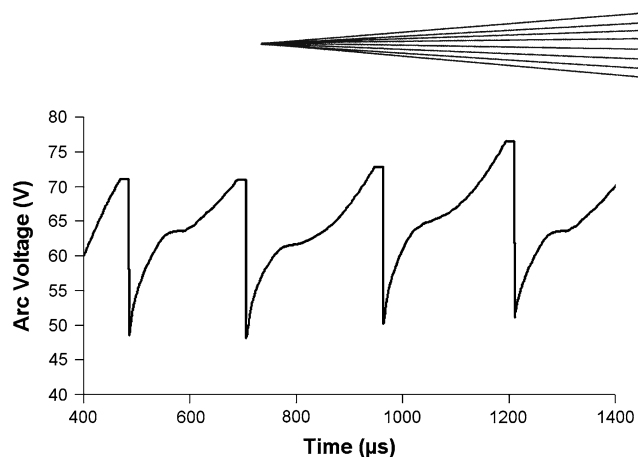

Fig. 1 Predicted time-evolution of arc voltage—reference case conditions

input to the gas as well as the temperature and velocity fields inside the torch. After validation of the predictions by comparison of the predicted and actual time-variation of arc voltage, the frequency, amplitude of arc fluctuations and space-distribution of the gas enthalpy in the exit plane of the torch were kept as reference data for the subsequent computations.

2. The computations of the time-variation of the temperature, velocity and concentration of plasma-forming gas *outside* the torch were, then, performed with the same voltage amplitude variation and enthalpy distribution in the exit plane of the torch as the ones predicted with the reference case conditions but with a fluctuation frequency multiplied by 3.

3. Finally, for the same arc fluctuation frequency as in the reference case, the amplitude of enthalpy variation was decreased so that it corresponded to a voltage fluctuation divided by 4.

4. Description of the Mathematical Model

4.1 Mathematical Model

Model assumptions: In this study, the transient and 3D model of the plasma jet issuing in ambient air is based on the following assumptions:

- Local thermodynamic equilibrium (LTE) prevails in the flow. This assumption is generally accepted in the modeling of atmospheric plasma jets because of the high elementary particles number densities that favour a strong collisional coupling for the exchange of energy between electrons and heavy particles, including chemical reactions such as ionisation and recombination (Ref 11). The medium is considered as a continuum, the plasma flow as a Newtonian fluid and the plasma gas as optically thin (Ref 12).

- Two gases are considered: the plasma gas and ambient air. In addition, it is supposed that no demixing effect and chemical reactions occurred in the gas phase.

- The gas flow is subsonic. Preliminary calculations have shown that, under the spraying conditions of the study, the Mach number is maximum inside the plasma torch and lower than 0.6.
- The turbulence phenomena are modeled using the Smagorinsky LES model (Ref 13) and the standard k–ε model.

Mathematical equations: The governing equations of the model are the conservation equations of mass, species, momentum, energy and turbulence that are written in 3D Cartesian coordinates and solved by using the commercial computational fluid dynamics (CFD) code *Code_Saturne*® *1.2.1* (Ref 14). The latter is a software package suitable for steady or unsteady, incompressible, dilatable, turbulent, multi-component reactive flows. It uses a numerical finite volume methods discretization applied to hybrid unstructured non-conformal and a multi-bloc mesh grid associated with the SIMPLEC algorithm with fourth-order numerical schemes.

The LES approach is implicitly filtered, meaning that the computational grid and discretization operators are considered as the filtering of the governing equations. The turbulent flow field is divided into grid-resolved and unresolved scales, where the unresolved scales must be modeled. The effect of the unresolved scales cannot be completely discarded and appears as an additional term in the 'filtered' Navier-Stokes equations involving the divergence of 'the sub-grid scale stress tensor.' To close the system of equations and solve it numerically, this additional unknown has to be modeled in terms of the other parameters. The most widely used model for the subgrid scale stress remains the Smagorinsky model that relates the sub-grid scale stress to the resolved strain rate tensor via an eddy viscosity μ_t. The essential difference between the LES and the k–ε models is that in the former model μ_t represents the dissipation due to the non-resolved part, whereas in the k–ε model it represents the dissipation of the whole spectrum of the fluctuating movement. In addition, the RANS approach involves time-averaging of the momentum equations and makes it possible to capture unsteady flow behaviour occurring over time scales at least an order of magnitude larger than the scales of the turbulent fluctuations.

The space-filtered non-stationary conservation equations used in the LES approach are the following:

- mass conservation:

$$\frac{\partial \rho}{\partial t} + \text{div}(\rho \bar{v}) = 0$$

- momentum conservation:

$$\frac{\partial (\rho \bar{v})}{\partial t} + \text{div}(\rho \bar{v} \otimes \bar{v}) = -\text{grad}(\bar{p}) + \rho g + \text{div}(\tau)$$

- energy conservation:

$$\frac{\partial (\rho \overline{H})}{\partial t} + \text{div}(\rho \bar{v}\overline{H}) = \text{div}\left[\left(\frac{\kappa}{C_p} + \frac{\mu_t}{Pr_t}\right)\text{grad}(\overline{H})\right]$$

- mass fraction conservation:

$$\frac{\partial (\rho m)}{\partial t} + \text{div}(\rho \bar{v}m) = \text{div}\left[\left(K_m + \frac{\mu_t}{Pr_t}\right)\text{grad}(m)\right]$$

where v, gas velocity; ρ, its density; t, time; p, pressure; g, gravity; τ, viscous strength tensor; C_p, gas-specific enthalpy; H, its mass enthalpy; κ, thermal conductivity; Pr_t, turbulent Prandtl number; m, mass fraction of species and K_m, molecular diffusivity. The species diffusion is assumed to be equal to the heat diffusion. As turbulent diffusion increases rapidly and becomes preponderant compared to the molecular one, this assumption is acceptable.

The viscous stresses tensor depends on the laminar and turbulent viscosity (μ_l and μ_t) and filtered strain rate tensor D

$$\tau = 2(\mu_l + \mu_t)D - \frac{2}{3}(\mu_l + \mu_t)\,\text{tr}(D)\text{I}_d$$

with $D = \frac{1}{2}\left(\frac{\partial \bar{v}_i}{\partial x_j} + \frac{\partial \bar{v}_j}{\partial x_i}\right)$ and $\mu_t = \rho(C\bar{\Delta})^2\sqrt{2DD}$ where $\text{tr}(D)$ is the trace of the matrix D, I_d the identity matrix, $\bar{\Delta}$ the filter width resulting of the finite volume discretization and $C = 0.18$, the Smagorinsky constant. The time-dependent velocity and enthalpy profiles at the plasma torch exit resulting from the MHD calculations of the arc dynamics inside the torch nozzle are used as input data for the boundary conditions at nozzle exit.

The boundary conditions for the turbulent energy k and its dissipation ε at the domain inlet are given by the following expressions: $k(r) = 0.5(I_t v(r))^2$, where I_t is the turbulent intensity set to 2% and $\varepsilon(r) = C_\mu k^2(r)/L_m$, where L_m is a mixing length expressed in terms of the torch radius as $L_m = 0.075\ R_{torch}$ and $C_\mu = 0.09$ (Ref 15).

The acceleration of droplets injected in the flow are calculated with a Lagrangian scheme assuming that they are punctual and spherical and do not collide with other droplets in the spray jet. The droplet break-up and evaporation are not considered in this study that deals essentially with the time-dependent phenomena at droplet injection. The droplet trajectory and velocity are determined from a force balance that involves gravity, buoyancy force, pressure gradient and drag forces.

Calculation domain for the plasma jet issuing from the plasma torch: The 3D calculation domain (Fig. 2) includes part of the torch nozzle (3 mm in length and 6 mm in diameter) in the internal field and the plasma free jet and substrate in the external field.

The latter is contained in a truncated cone 100 mm high, radius of the small base 48 mm and of the large base 72 mm. The liquid injector is located at 8 mm downstream of the torch exit and 12 mm above the plasma axis. The numerical grid consists of 187,200 nodes with a finer mesh close to the walls to provide for an accurate calculation of the heat flux.

5. Results and Discussion

5.1 Flow Behaviour

Figures 3-5 show the time-dependent predictions of the flow behaviour performed with the 'reference' torch operating conditions and the LES turbulence model. They represent a 5,000-K isotherm (chosen for a convenient visualisation) colored by the mass fraction of plasma gas, gas momentum flux ($\rho.v^2$) and total (molecular plus turbulent) viscosity of the plasma flow, respectively, in the x–y injection plane. The latter is parallel to the plane of the nozzle exit and contains the injector axis.

Figure 3 clearly reveals (i) the hot puffs of the plasma gas traveling with the flow at the same frequency as arc fluctuations and (ii) the rotation of the plasma jet due to the rotation of the arc attachment on the anode wall because of the vortex injection of the plasma-forming gas. The length of the plasma jet, defined by the 5,000-K isotherm, fluctuates between 50 and 100 mm.

Figures 4 and 5 also show that the two key parameters that condition the precursor injection in the plasma flow (gas momentum density and total viscosity) are continuously varying in the particle injection zone, due to the variation in the length of the electric arc and location of the anodic arc root. As the droplet momentum imparted
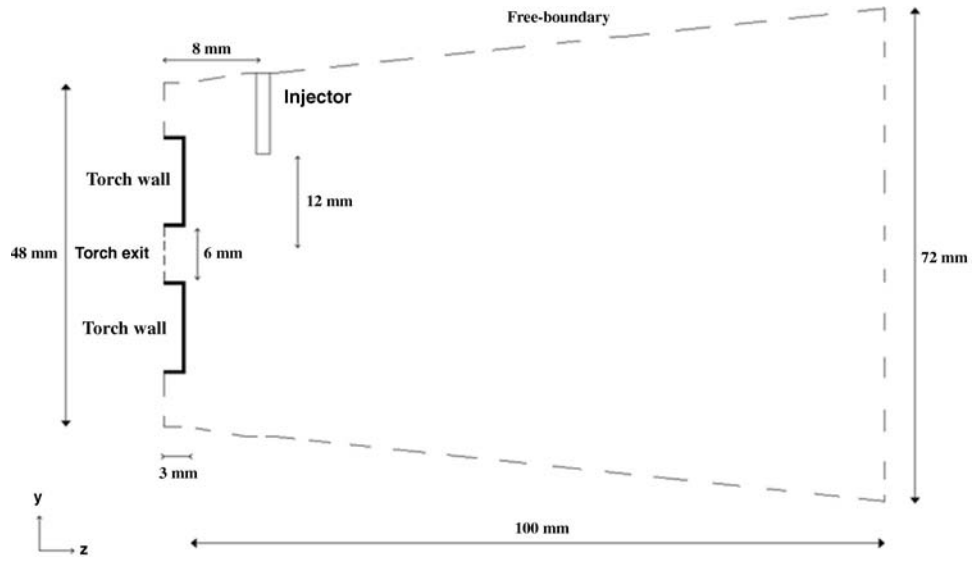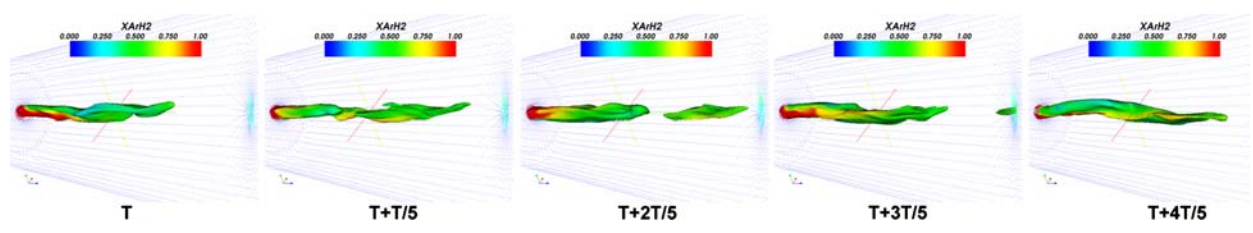

Fig. 2 Calculation domain

Fig. 3 5,000-K isotherm colored by the mass fraction of plasma gas at five different step times (T, $T + T/5$, $T + 2T/5$, $T + 3T/5$, $T + 4T/5$ where T is the arc fluctuation period)—reference case conditions
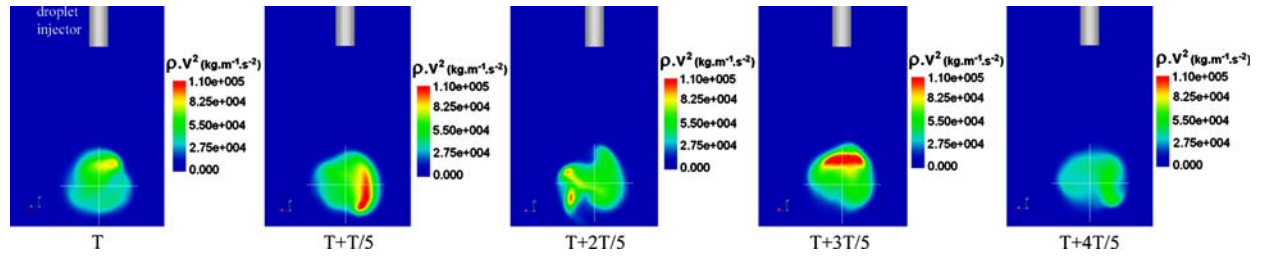

Fig. 4 Momentum flux (kg m^{-1} s^{-2}) in the droplet injection plane at five different step times (T, $T + T/5$, ...)—reference case conditions

by the carrier gas cannot follow the arc root fluctuations, the droplet trajectories fluctuate accordingly.

The maximum molecular viscosity is located near the axis of the plasma jet where the highest temperatures prevail, whereas the maximum turbulent viscosity that results from the gas flow shearing is located at the periphery of the jet and about twice greater.

Figure 6 shows the predicted gas velocity and temperature along the torch axis given by both turbulence models used in this study as well as experimental measurements (Ref 15). Predictions are averaged over four periods of the arc fluctuations. It should be noticed that with the k–ε model, the turbulence proceeds suddenly at about 1.5 cm from the torch exit, whereas with the LES model, it proceeds more regularly. The time-averaged projections from both models show reasonable agreement with experiments. The predictions achieved with the k–ε should probably be improved by adjusting the level of turbulence intensity at the nozzle exit and constants of the model to delay and modify the turbulence development.

5.2 Droplet Injection

Figure 7 shows the trajectories, in the y–z plane, of droplets injected at three different instants of the arc fluctuation period T. It should be noted that as the droplet break-up and evaporation are not taken account in this study, only the first part of the trajectories are representative of the droplet actual behaviour. Droplets with diameter of 20, 40 and 60 μm were introduced at the same time and point of the calculation domain (see Fig. 2) with an initial radial velocity of 30 m s^{-1}.

As experimentally observed and as expected, the penetration of the larger droplets in the plasma jet is easier than for the smaller ones, at least in the penetration zone. Also, the larger droplets are less affected by the plasma fluctuations than the smaller droplets. It must be noted that, due to their low mass inertia, the 10-μm droplets do not penetrate the plasma jet with the specified injection velocity whatever the instant of injection. In addition, even if the droplets are injected at the same time, their
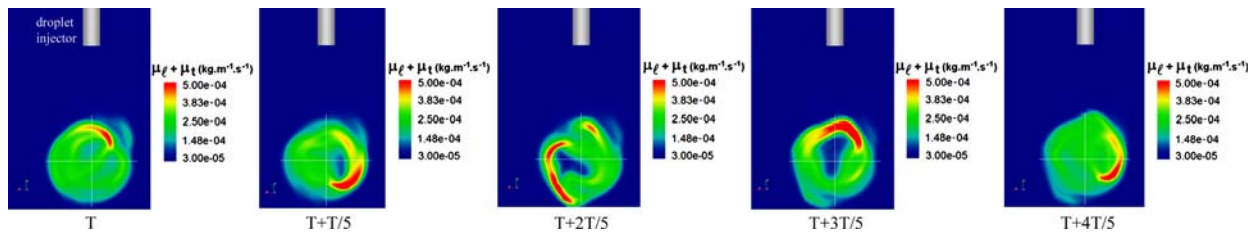

Fig. 5 Total viscosity in the droplet injection plane (kg m^{-1} s^{-1}) at five different step times (T, $T + T/5$, ...)—reference case conditions
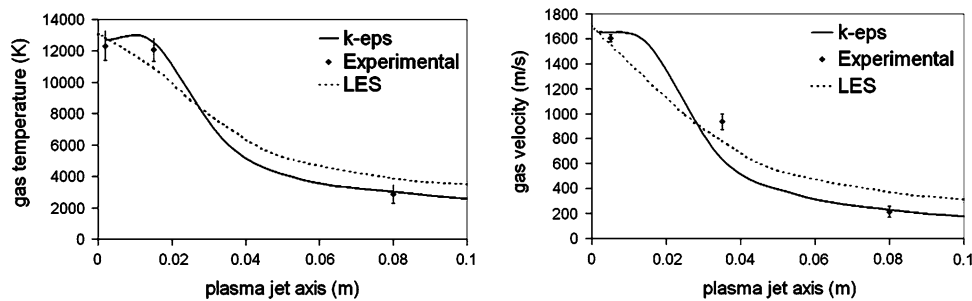

Fig. 6 Time-averaged evolution of predicted and measured gas velocity and temperature along the torch axis
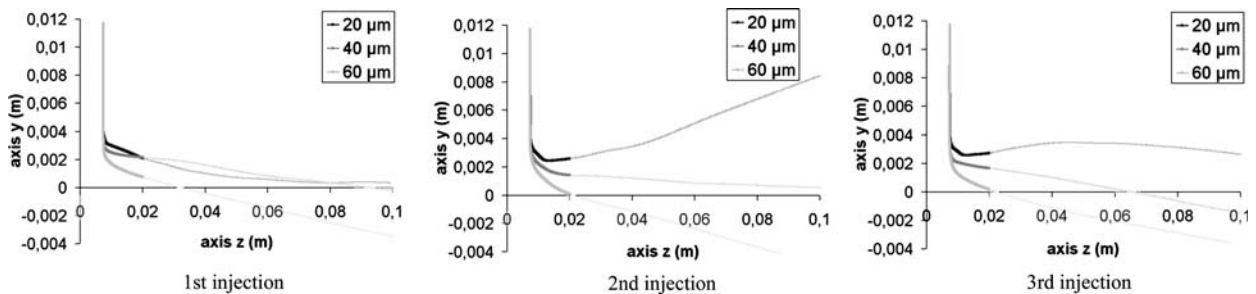

Fig. 7 Droplet trajectories in the y–z plane—reference case conditions
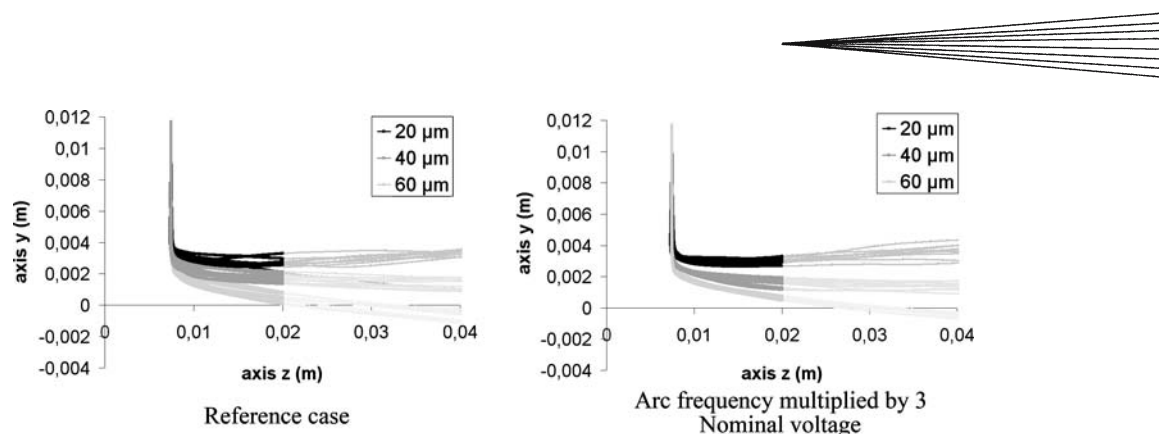
Fig. 8 Effect of arc fluctuation parameters on droplet trajectories

dwell time will depend on their size and also place where they penetrate the plasma jet. Therefore, they can see different turbulence level and be embedded in different eddies. This may explain that the 40-μm droplet trajectory is not located between the trajectories of the 20- and 60-μm droplets.

The width of the droplet spray jet changes between 1.5 and 2.5 mm at 20 mm from the plasma torch exit; this variation is mainly due to the combine effects of the time-variation of the plasma jet momentum and viscosity. In addition, the size of the fragmented droplets that is controlled by the plasma jet momentum will depend on the instant of injection.

5.3 Influence of Arc Fluctuation Frequency and Amplitude on Particle Behaviour

Figure 8 shows the effect on droplet trajectories, of an increase by a factor 3 of the arc fluctuation frequency. Each graph corresponds to different droplet sizes and instants of injection.

It should be noted, for a droplet with a given size, that

- an increase in the arc fluctuation frequency brings about a lower droplet dispersion, and
- a decrease of the arc voltage fluctuation amplitude also results in a lower dispersion of the droplet spray jet.

As expected, both effects are more marked for the small droplets.

6. Conclusion

Plasma spraying using liquid feedstock involves intricate interactions between the fluctuating gas jet and injected droplets. They result in time-dependent droplet parameter distributions. The development of realistic models can help to get a better understanding of these complex interactions and also to define an operating window to improve the injection and treatment of liquid precursors. In this study, 3D numerical models have been used to examine the influence of the arc voltage fluctuation amplitude and frequency on the time-evolution of the plasma jet flow fields and droplet injection. They involved arc dynamics inside the plasma torch, time-behaviour of

the plasma jet issuing in the ambient air and droplet injection. They have made it possible to predict the time-variation of the plasma jet density momentum and viscosity in the plane where the precursor droplets are injected. They have also showed, as experimentally observed, that high arc fluctuation frequency and low-voltage amplitude fluctuation result in a less dispersed spray jet and a more homogeneous thermal treatment, for a given particle size.

The developments in hand relate to (i) the effect of grid refinement and Smagorinsky constant value on the turbulence development predicted by the LES model, (ii) the use of more space-resolved velocity and enthalpy boundary conditions at the nozzle exit for the plasma jet model and (iii) to the coupling of the models of droplet fragmentation and evaporation with the non-stationary behaviour of the flow.

References

1. C.C. Berndt, A.H. King, T. Chraska, and J. Karthikeyan, Plasma Spray Synthesis of Nanomaterials, http://www.matscieng.sunysb.edu/ctsr/nuggets/nugget1/index.html, 1997
2. P.F. Blazdell and S. Kuroda, Plasma Spraying of Submicron Ceramic Suspensions Using a Continuous Ink Jet Printer, *Surf. Coat. Technol.*, 2000, **123**, p 239-246
3. C. Delbos, Understanding the Injection of Metal or Ceramics Suspensions in a DC plasma jet, Ph.D Thesis, in French, University of Limoges, France, 2004
4. R. Etchart-Salas, V. Rat, J.F. Coudert, P. Fauchais, and G. Lafougère, Influence of Arc Instabilities on the Injection in Suspension Plasma Spraying, *High Technol. Plasma Processes*, 2006, **9**, May 29-June 4 (St-Petersburg, Russia)
5. A. Ozturk and B.M. Cetegen, Modeling of Plasma Assisted Formation of Precipitates in Zirconium Containing Liquid Precursors Droplets, *Mater. Sci Eng.*, 2004, **A384**, p 331-351
6. L. Xie, X. Ma, E.H. Jordan, N.P. Padture, and M. Gell, Deposition of Thermal Barrier Coatings Using the Solution Precursor Plasma Spray Process, *J. Mater. Sci.*, 2004, **39**, p 1639-1646
7. J. Oberste Berghaus, S. Bouaricha, J.G. Legoux, and C. Moreau, Injection Conditions and in-flight Particles States in Suspension Plasma Spraying of Alumina and Zirconia Nano-ceramics, *Thermal Spray 2005: Advances in Technology and Application*, ASM International, 2005, May 2-4 (Basel, Switzerland), ASM International
8. M. Gell, Application Opportunities for Nanostructured Materials and Coatings, *Mater. Sci. Eng.*, 1995, **A204**, p 246-251
9. R. Benocci, R. Florio, A. Galassi, M. Paolicchio, M. Piselli, C. Sala, M. Sciascia, and E. Sindoni, Experimental Study for the Optimization of Plasma Torch Operations, *Eur. Phys. J.*, 1999, **D6**, p 269-279

10. E. Moreau, C. Chazelas, G. Mariaux, and A. Vardelle, Modeling the Restrike Mode Operation of a DC Plasma Spray Torch, *J. Thermal. Spray Technol.*, 2006, **15**(4), p 524-530
11. N. Singh, M. Razafinimanana, and A. Gleizes, The Effect of Pressure on a Plasma Plume: Temperature and Electron Density Measurements, *J. Phys. D: Appl. Phys.*, 1998, **31**, p 2921-2928
12. M. Boulos, P. Fauchais, and E. Pfender, Thermal Plasmas: Fundamental and Applications, Vol. 1. Plenum Press, New York, 1994, p 33-43
13. P. Sagaut, Introduction to Large Eddy Scale Simulations for the Modeling of Uncompresible Flows, in French, *Mathématiques et Applications*, 1998, Vol. 30, Springer-Verlag
14. F. Archambeau, N. Méchitoua, and M. Sakiz, Code_Saturne: A Finite Volume Code for the Computation of Turbulent Incompressible Flows—Industrial Applications, *Int. J. Finite Vol.*, 2004, **1**(1), p 1-62
15. G. Mariaux and A. Vardelle, 3-D Modeling of the Plasma Spray Process. Part: 1 Flow Modeling, *Int. J. Therm. Sci.*, 2005, **44**, p 357-366